Microstructure and property of TiB-reinforced Ti alloy composites by laser metal deposition

Yunlu Zhang[a], Jingwei Zhang[a], Frank Liou[a], Joseph Newkirk[b]

[a]Department of Mechanical Engineering, Missouri University of Science and Technology, Rolla, MO 65409
[b]Department of Material Science and Engineering, Missouri University of Science and Technology, Rolla, MO 65409

REVIEWED

Abstract

TiB-reinforced Ti alloy composites have been laser deposited with pre-alloyed Ti-6Al-4V-1B powder. The microstructure of the as-deposited and heat treated composites have been characterized in detail using scanning electron microscope (SEM). A homogeneous dispersion of needle-like TiB precipitates is formed in the Ti-6Al-4V α/β matrix. TiB precipitates promote formation of small near equaxed α/β grain after β annealing process. The micro-hardness of the laser deposited composites increase 20-30% with 5 vol. % TiB precipitates compared to unreinforced Ti-6Al-4V deposits.

Introduction

Titanium alloy/TiB reinforced composites have been widely studied during the last few decades [1–8] because they combine the high stiffness and strength from boride and the toughness from the titanium alloy matrix. The high compatibility of thermal expansion coefficient and density of titanium and titanium boride results in low thermal stress and thus low probability of cracking during manufacturing.

Besides casting[6] and sintering[5], laser metal deposition (LMD) is one of the methods that have been developed to manufacture titanium alloy TiB composites. The merit from additive manufacturing makes LMD easily fabricate the near-net shape FGM part with varied compositions at different locations that is hard to archive by other methods.

In general, boron precursor could be introduced in the Ti alloy system in three ways: elemental boron B, titanium diboride TiB_2, and pre-alloyed Ti-B powder. The first two powders need to be mixed with adequate amount of Ti powder before deposition. This is the method adopted in research before[1,3,4,8]. B and TiB_2 powders are often irregular in shape and its size is too small that may produce problems in the transporting system. The melting temperature of ceramic TiB_2 powder is 3500K, and it may not be melted at low energy density condition. The spherical pre-alloyed Ti-B powder has the best flowability among these powders. Lieberman et al.[9] sintered gas atomized Ti–6Al–4V–1B to reconstruct the 3D morphology of TiB whiskers. But no research about laser deposited pre-alloyed powder has been conducted and studied to date.

In the present research, the relationship between microstructure, hardness, and process parameters of Ti-6Al-4V/TiB composites by gas atomized pre-alloyed Ti-6Al-4V-1B powder were studied. The influences of β annealing on the deposits were also addressed.

Experiment

IPG photonics 1kW Nd:YAG fiber laser with a wavelength of 1064 nm and a powder feeder from Baystate Technologies were used in the laser deposition system. The beam size was 3 mm. All depositions were conducted in a protective argon atmosphere at a flow rate of 20 L/min. Ti-6Al-4V alloy substrates were used for depositing Ti-6Al-4V/TiB composites and their dimensions are 2 ×1/2 ×1/4 inch.

The material used in this work is gas atomized Ti-6Al-4V-1B powder (-100/+325 mesh, ATI powder metals). Its chemical analyzed composition is shown in Table 1. 1 wt. % B is less than the eutectic point 1.64 wt. % in Ti-B phase diagram, therefore 5 vol. % TiB would form in the matrix in theory. As illustrated in Figure 1(a), the majority of the gas atomized powders are spherical which is good for flowability. Fine TiB precipitates exhibit an acicular (needle-like) morphology with a length less than 10 μm and a width less than 0.4 μm in Figure 1(b). TiB needles decorate the prior-β grain boundary that indicates the size of prior-β grain is around 10 μm. When these fine features in the powder dissolve in the melt pool, the boron concentration is evenly distributed at 10 μm level.

Table 1: Chemical analyzed composition of gas atomized Ti-6Al-4V-1B powder

	Al	V	B	Fe	C	O	N	Ti
Wt.%	6.43	4.13	1.05	0.074	0.053	0.148	0.038	Bal.

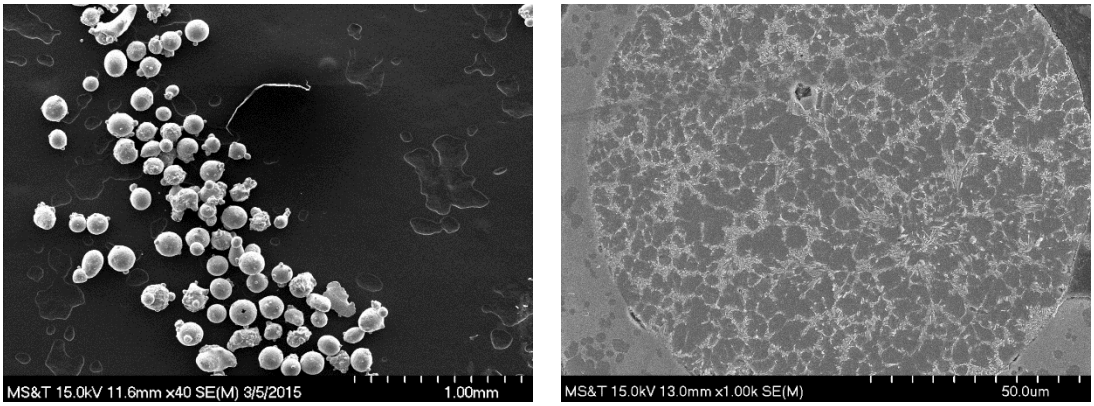

(a) (b)

Figure 1: Secondary scanning micrograph of Ti-6Al-4V-1B powders. (a) particle shape and morphology and (b) cross section view of one particle

TiB_2 powders (-325 mesh, Cerac Inc.) were mixed with adequate amounts of Ti-6Al-4V and pure Ti powders to get nominal 1 wt. % boron for comparison. The TiB_2 powders have irregular shape and non-uniform size as shown in Figure 2. In addition, Ti-6Al-4V powder deposits were also prepared.

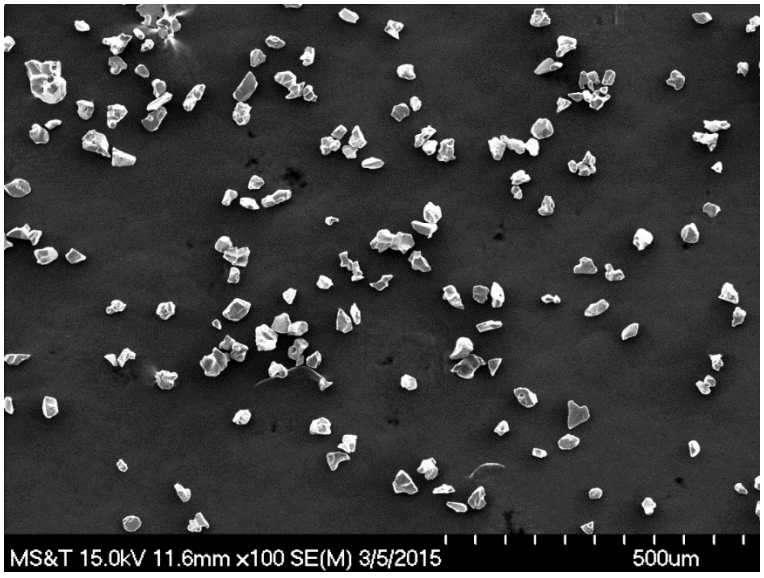

Figure 2: Secondary scanning micrograph of TiB2 powders

To study the influence of process parameters on microstructure and property, 3 combinations of laser power and scan speed were chosen for each powder set. All the deposited thin walls were 3 layers and 20 mm long. After deposition, specimens were β annealed at 1100 ℃ for 1 h followed by air cooled (AC) or furnace cooled (FC). Powder compositions, sample nomenclatures, process parameters and energy density used are listed in Table 2.

Table 2: Sample nomenclature, powder composition, process parameters and laser density

Nomenclature	Powder composition	Power, P (W)	Scan speed, v (mm/min)
Ti64-900/300	Ti-6Al-4V	900	300
Ti64-600/300	Ti-6Al-4V	600	300
Ti64-900/450	Ti-6Al-4V	900	450
Ti64B-900/300	Ti-6Al-4V-1B	900	300
Ti64B-600/300	Ti-6Al-4V-1B	600	300
Ti64B-900/450	Ti-6Al-4V-1B	900	450
TiB2-600/300	Ti-6Al-4V+TiB_2+Ti	600	300

The specimens were cut by electrical discharge machining to reveal their central cross sections, and then mounted, ground and polished per metallography standards. The SEM characterization was performed by using the Hitachi 4700 scanning electron microscope. Vickers hardness was measured (Struers Duramin5 tester) on these samples using a 9.81 N load for 10 s across the deposits height. Hardness measurements were taken in triplicate and averaged.

Results and discussion

Microstructure analysis

Figure 3 shows macrostructure of Ti-6Al-4V, Ti-6Al-4V-1B, and TiB_2 mixed powder deposits respectively. One distinctive feature of the Ti-6Al-4V deposit is the acicular martensite inside large prior-β grains. The prior β-grains changed from fine equiaxial grains in the melt pool and heat affected zone into large columnar grains in the deposits as shown in Figure 3(a).

Large prior β-grains are known to degrade strength, ductility, and fatigue resistance[10]. In comparison, the boron containing samples (not limited to Ti64B-900/300 and TiB2-900/300) show no obvious prior β-grain and the structure is highly uniform at macrostructure level. A distinctive boundary is clear in the samples containing boron that indicate the depth of first melt pool.

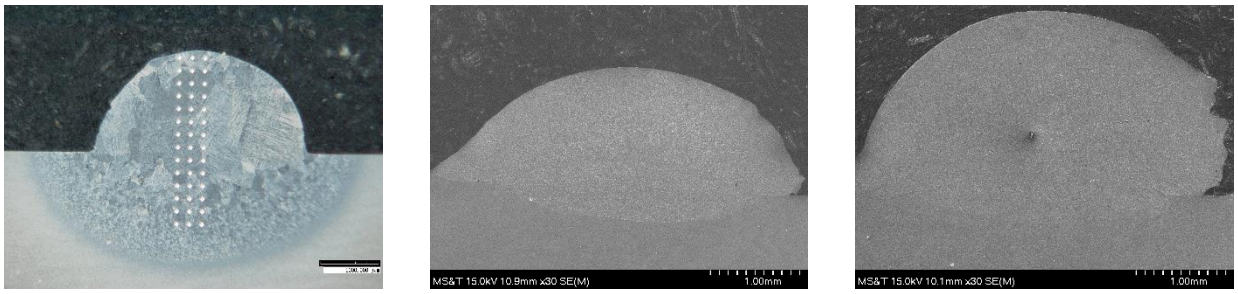

(a) (b) (c)

Figure 3: Full view image of deposits: (a) Ti64-900/300, (b) Ti64B-900/300, and (c) TiB2-900/300

Figure 4 illustrates the microstructure of Ti64B-900/300 at as deposited, air cooled, and furnace cooled states and Ti64-900/300 at air cooled and furnace cooled states. TiB precipitates stand out from the Ti-6Al-4V matrix as white needles in the secondary electron images as shown in Figure 4(a-c). The lengths of these precipitates are in the range of 5-25 μm. While some needles are extremely short (less than 2 μm), it is likely that the cross-section of a needle lies perpendicular to the view plane. The needles formed small clusters that were oriented in similar directions, but the needles distribute evenly and orientate randomly at the hundred micron level. The fine martensite structure of the matrix in the as deposited state changes into thick α/β laths after the β annealing process, while TiB precipitates do not change significantly. There is known orientation relationship between TiB and α[11] indicating that TiB precipitates promote the near equiaxed α to nucleate and grow upon slow cooling from above the β-transus temperature[6]. The existence of fine distributed precipitates also limits α grains from growing into long laths. The aspect ratio of the α lath of the air cooled specimen in Figure 4(b) is slightly larger than the furnace cooled specimen in Figure 4(c) due to the cooling rate being slower in the latter one. The air cooled and furnace cooled Ti-6Al-4V deposits show large α colonies with grain boundary α in Figure 4(d-e) that is harmful for strength, ductility, and fatigue resistance[12].

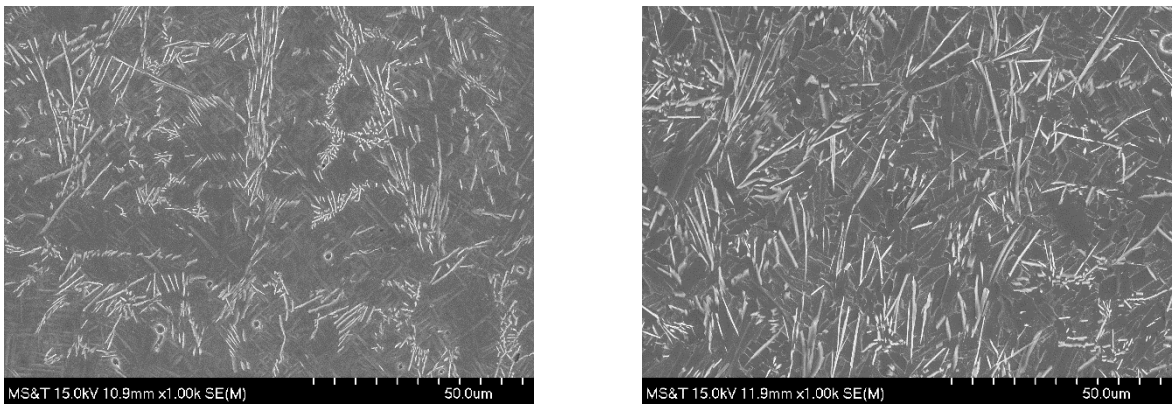

(a) (b)

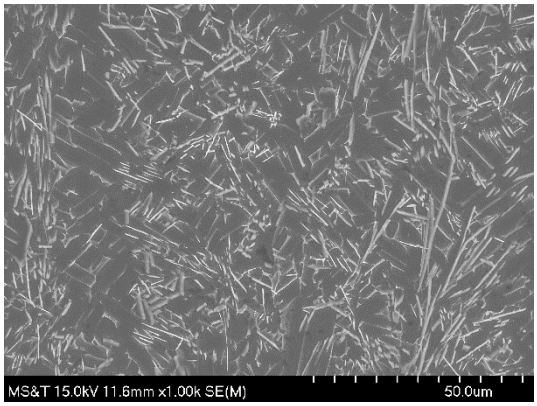

(c)

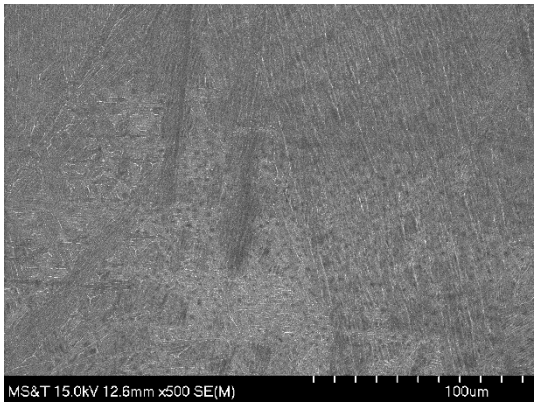

(d)

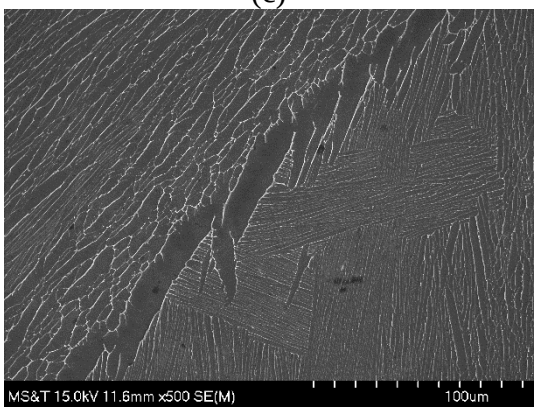

(e)

Figure 4: SEM micrograph of deposits: (a) Ti64B-900/300, (b) Ti64B-900/300AC, (c) Ti64B-900/300FC, (d) Ti64-900/300AC, and (e) Ti64-900/300FC

Incompletely dissolved Ti-6Al-4V and TiB_2 particles were observed in several locations of the samples containing TiB_2 as shown in Figure 5. This phenomenon indicated insufficient heat input for this powder system.

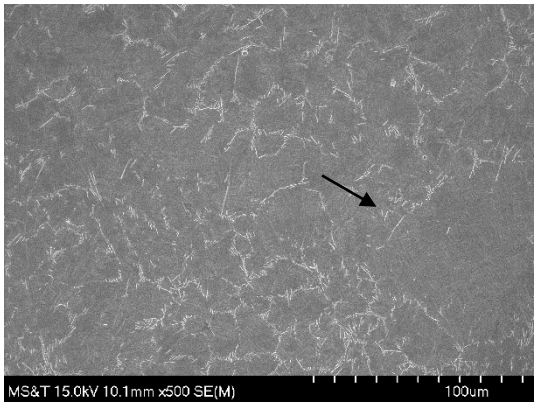

(a)

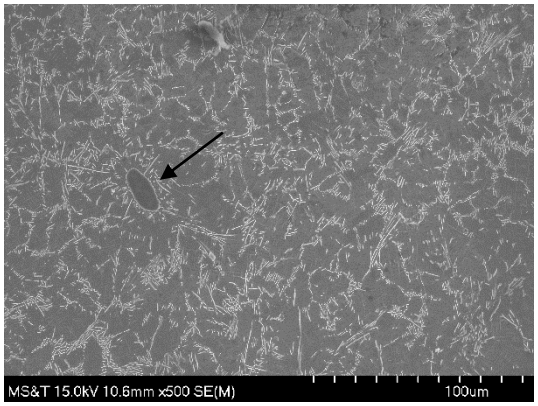

(b)

Figure 5: Incomplete dissolved particle observed: (a) Ti6Al-4V particle in TiB2-600/300, (b) TiB_2 particle in TiB2-600/300

Hardness analysis

The micro hardness distribution of the deposits on the central cross sections was tested. A typical distribution is illustrated in Figure 6. The hardness is fairly stable above 0.5 mm. Therefore, the hardness of different specimens was measure at the location 0.6 mm below the top of the deposit as summarized in Table 3. In general, with 1 wt. % B addition and 5 vol. % TiB formed, hardness of the deposits increased 100-140 HV at all three states. The hardening effect is mostly contributed by hard precipitates TiB due to the fact that solubility of boron in the Ti-matrix is extremely low, meaning almost no solution hardening is expected. It also should be noted that the hardness drops 30-50 HV after the β-annealing process, which is attributed to the formation of near equaxed α grains.

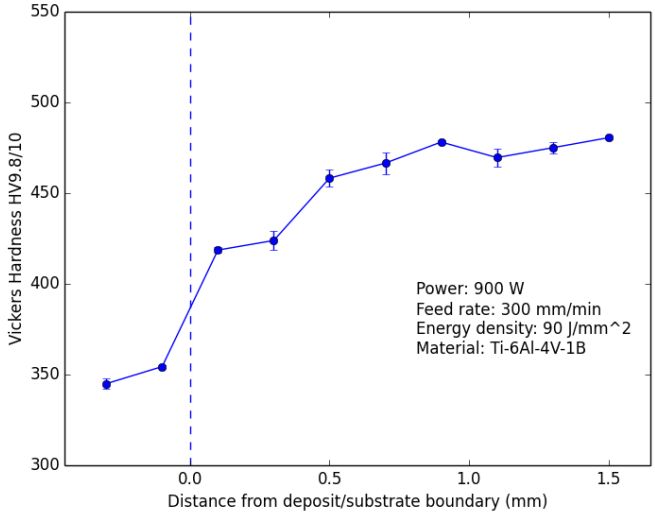

Figure 6: Micro hardness distribution of TiB2-900/300. The error bar represents standard deviation of 3 measurements at the same height.

Table 3: Micro hardness of specimens at as deposited, air cooled, and furnace cooled state measured at 0.6 mm below the top of deposit

	Ti64-900/300	Ti64-600/300	Ti64-900/450	Ti64B-900/300	Ti64B-600/300	Ti64B-900/450
As deposited	378	397	381	478	523	472
Air cooled	342	370	353	444	466	425
Furnace Cooled	339	336	338	447	473	433

Conclusion

Using laser metal deposition process, the Ti-6Al-4V/TiB composite has been successfully fabricated by using gas atomized pre-alloyed Ti-6Al-4V-1B powder. The TiB needles distribute evenly and orientate randomly as small clusters in the deposits. Large prior-β grains have been eliminated in samples containing boron. TiB precipitates limit the formation of long needle in martensite and promote the generation of near equaxed α/β grain after the β annealing process. These changes in microstructure are beneficial for strength, ductility, and fatigue resistance[10]. The incompletely dissolved powder phenomena shown in mixed powder deposits did not appear in pre-alloyed powder deposits. Furthermore, the microhardness of the samples containing boron increases 20-30% compared to Ti-6Al-4V deposits.

Acknowledgements

The authors would like to express their sincere gratitude to Karen M. Brown Taminger and William J. Seufzer for their helpful inputs. This work has been supported from National Aeronautics and Space Administration EPSCoR program (Grant# NNX13AM99A).

References

1] Banerjee R., Collins P. C., Genç A., and Fraser H. L., 2003, "Direct laser deposition of in situ Ti–6Al–4V–TiB composites," Mater. Sci. Eng. A, **358**(1–2), pp. 343–349.

[2] Kooi B. ., Pei Y. ., and De Hosson J. T. ., 2003, "The evolution of microstructure in a laser clad TiB–Ti composite coating," Acta Mater., **51**(3), pp. 831–845.

[3] Galvan D., Ocel ḱ V., Pei Y., Kooi B. J., De Hosson J. M., and Ramous E., 2004, "Microstructure and properties of TiB/Ti-6Al-4V coatings produced with laser treatments," J. Mater. Eng. Perform., **13**(4), pp. 406–412.

[4] Wang F., Mei J., and Wu X., 2008, "Direct laser fabrication of Ti6Al4V/TiB," J. Mater. Process. Technol., **195**(1–3), pp. 321–326.

[5] Panda K. B., and Ravi Chandran K. S., 2003, "Titanium-titanium boride (Ti-TiB) functionally graded materials through reaction sintering: Synthesis, microstructure, and properties," Metall. Mater. Trans. A, **34**(9), pp. 1993–2003.

[6] Hill D., Banerjee R., Huber D., Tiley J., and Fraser H. L., 2005, "Formation of equiaxed alpha in TiB reinforced Ti alloy composites," Scr. Mater., **52**(5), pp. 387–392.

[7] Bermingham M. J., Kent D., Zhan H., StJohn D. H., and Dargusch M. S., 2015, "Controlling the microstructure and properties of wire arc additive manufactured Ti–6Al–4V with trace boron additions," Acta Mater., **91**, pp. 289–303.

[8] Genç A., Banerjee R., Hill D., and Fraser H. L., 2006, "Structure of TiB precipitates in laser deposited in situ, Ti-6Al-4V–TiB composites," Mater. Lett., **60**(7), pp. 859–863.

[9] Lieberman S. I., Gokhale A. M., and Tamirisakandala S., 2007, "Reconstruction of three-dimensional microstructures of TiB whiskers in powder processed Ti–6Al–4V–1B alloys," Mater. Charact., **58**(6), pp. 527–533.

[10] Lütjering G., 1998, "Influence of processing on microstructure and mechanical properties of (α+ β) titanium alloys," Mater. Sci. Eng. A, **243**(1), pp. 32–45.

[11] Hill D. M., 2006, "Microstructure and mechanical properties of titanium alloys reinforced with titanium boride."

[12] Bontha S., 2006, “The Effect of Process Variables on Microstructure in Laser-Deposited Materials.”